Available online at www.sciencedirect.com
SCIENCE DIRECT®
Journal of Organometallic Chemistry 690 (2005) 3886–3897
Journal of Organo metallic Chemistry
www.elsevier.com/locate/jorganchem

The variation of coordination modes of aromatic imines in iron carbonyl complexes: Is there a correlation between bond lengths in organometallic model compounds and the reactivity of the ligands in catalytic C–C bond formation reactions?

W. Imhof *, A. Göbel, L. Schweda, D. Dönnecke, K. Halbauer

Institute of Inorganic and Analytical Chemistry, Friedrich-Schiller-University, August-Bebel-Str. 2, 07743 Jena, Germany

Received 1 April 2005; received in revised form 18 April 2005; accepted 18 April 2005
Available online 28 June 2005

Abstract

The reaction of aromatic imines with $Fe_2(CO)_9$ proceeds via a two-step reaction sequence. A C–H activation reaction in *ortho*-position with respect to the exocyclic imine function is followed by an intramolecular hydrogen transfer reaction towards the former imine carbon atom. The resulting dinuclear iron carbonyl complexes show an aza-ferra-cyclopentadiene ligand which is apically coordinated by the second iron tricarbonyl moiety. Comparing the bond lengths of 43 different compounds, which were synthesized and structurally characterized in our group shows that the iron iron bond length correlates with one of the iron carbon bond lengths. The longer the iron carbon bond between the apically coordinated iron atom and the carbon atom next to the former imine carbon atom is, the shorter is the iron iron bond. The same ligands may be used as the substrates in ruthenium catalyzed C–C bond formation reactions. Whereas most of the imines react via the formal insertion of CO and/or ethylene into the C–H bond in *ortho*-position to the imine function, the ligands that show the longest iron carbon bond lengths in the model compounds under the same reaction conditions produce different types of isoindolones.

Keywords: Iron; Carbonyls; C–H activation; Catalysis; X-ray

1. Introduction

The reaction of aromatic imines with $Fe_2(CO)_9$ or $Fe_3(CO)_{12}$, respectively, leads to the formation of dinuclear iron carbonyl complexes via the activation of a C–H bond in *ortho*-position with respect to the exocyclic imine function followed by an intramolecular hydrogen shift reaction towards the former imine carbon atom. The resulting organometallic compounds therefore consist of an formally six electron donating enyl-amido ligand adopting a μ_2-η^3-coordination mode (Scheme 1) [1–14]. This reaction sequence has been shown to be the major reaction pathway for a wide variety of carbocyclic and heterocyclic imine ligands.

The iron carbonyl complexes mentioned above may well serve as model compounds for the initial steps in ruthenium catalyzed C–H activation reactions of aromatic compounds taking place in *ortho*-position with respect to exocyclic functional groups with potential metal coordinating donor sites. These catalytic C–H activation reactions are used to introduce new carbon carbon bonds instead and due to the initial cyclometallation step show the same regioselectivity as the stoichiometric reactions with iron carbonyls [15–31].

The results presented herein show that the coordination mode of the ligand represented by the various bond

* Corresponding author. Tel.: +49 3641 94 8129; fax: +49 3641 94 8102.
E-mail address: Wolfgang.Imhof@uni-jena.de (W. Imhof).

0022-328X/$ - see front matter
doi:10.1016/j.jorganchem.2005.04.056

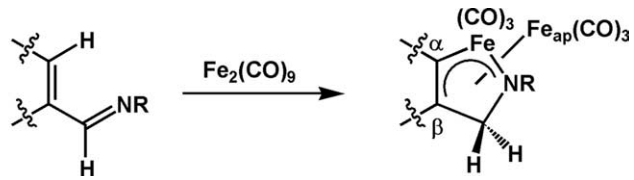

Scheme 1.

lengths may change dramatically depending on the aromatic system the imine ligands are based upon. In addition, these findings are used to attempt a correlation between the properties of the coordination of the imine ligands in organometallic compounds with the reaction pathways observed in catalytic C–C coupling reactions.

2. Results and discussion

During the last years, we have published a number of diironhexacarbonyl complexes of various aromatic imines which are produced via the reaction depicted in Scheme 1 [5,6,9–12]. The imine ligands are easily prepared by condensation of the corresponding aromatic aldehyde with a primary amine (cf. Section 3).

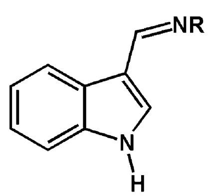

1: R = Ph

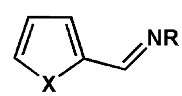

2: R = Ph, X = S
3: R = Cy, X = S
4: R = Ph, X = NMe
5: R = Cy, X = NMe
6: R = Fc, X = NMe
7: R = Fur, X = NMe
8: R = Cy, X = O

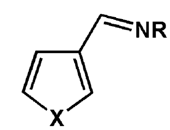

9: R = 4-$SiMe_3$-C_6H_4,
X = S

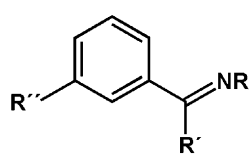

10: R = Ph, R´ = R`` = H
11: R = Cy, R´ = R`` = H
12: R = 4-Br-C_6H_4, R´ = R`` = H
13: R = 4-CF_3-C_6H_4, R´ = R`` = H
14: R = Cy, R´ = Me, R`` = H
15: R = Phe, R´ = R`` = H
16: R = Met, R´ = R`` = H
17: R = N=C(H)-(3-Cl-C_6H_4),
R´ = H, R`` = Cl

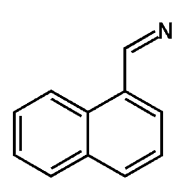

18: R = Ph
19: R = Cy
20: R = H
21: R = N=C(H)-$C_{10}H_7$

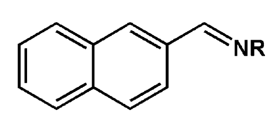

22: R = Ph
23: R = Cy

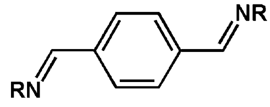

24: R = Ph
25: R = Cy

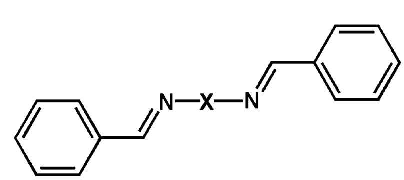

26: X = C_6H_4
27: X = C_6H_{10}-S-C_6H_{10}
28: X = C_6H_{10}-O-C_6H_{10}
29: X = C_6H_{10}-CH_2-C_6H_{10}
30: X = C_6H_{10}
31: X = C_6H_{10}-CH_2-C_6H_{10}

Scheme 2.

Scheme 2 shows the different classes of aromatic imines used in this investigation. The ligands **1**–**9** are based on heteroaromatic aledehydes like 3-indolecarbaldehyde, thiophene-2-carbaldehyde, *N*-methylpyrrole-2-carbaldehyde, furan-2-carbaldehyde and thiophene-3-carbaldehyde. **10**–**23** are benzaldehyde or α- or β-naphthylcarbaldehyde derivatives whereas **24**–**31** are bifunctional imines produced from terephthalic aldehyde (**24**, **25**) or from various diamines (**26**–**31**).

The synthesis and X-ray structures of the dinuclear iron carbonyl compounds prepared from these imines have been published before with the exception of the molecular structures of the iron carbonyl complexes synthesized from **7**, **8**, **14** and **30**. The synthesis of the corresponding iron carbonyl compounds **32**–**35** as well as the synthesis of the new but not structurally characterized di- and tetranuclear compounds **36**–**38** is shown in Scheme 3.

The molecular structures of **32**–**35** are presented in Figs. 1, 3, 5 and 7, respectively. They all show the coordination mode which is typical for this class of compounds, in which a diironhexacarbonyl fragment is bound to an enyl-amido ligand in a μ_2-η^3-fashion. The molecular structures of these four iron carbonyl compounds already show, that most of the bond lengths in the coordination polyhedra of the iron atoms are very similar in **32**–**35**. The most important exception from this finding is the bond length between the apical iron atom Fe_{ap} and the carbon atom (C_β in Scheme 1) next to the methylene group which was formed by the hydrogen transfer reaction. This iron carbon bond length

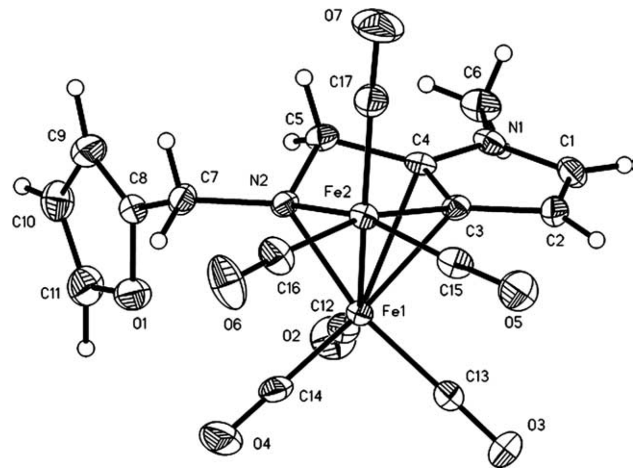

Fig. 1. Molecular structure of **32**, selected bond lengths (pm) and bond angles (°): Fe1–Fe2 241.6(1), Fe1–N2 195.6(3), Fe1–C3 214.2(4), Fe1–C4 243.8(4), Fe2–N2 199.2(3), Fe2–C3 197.4(4), C3–C4 140.6(5), C4–C5 147.6(5), C5–N2 148.3(5); N2–Fe1–Fe2 52.94(9), N2–Fe1–C3 74.5(1), N2–Fe1–C4 61.0(1), Fe2–Fe1–C3 50.9(1), Fe2–Fe1–C4 71.1(1), C3–Fe1–C4 35.0(1), N2–Fe2–C3 77.6(1), Fe2–C3–C4 112.2(2), C3–C4–C5 118.6(3), C4–C5–N2 100.0(3), C5–N2–Fe2 112.9(2).

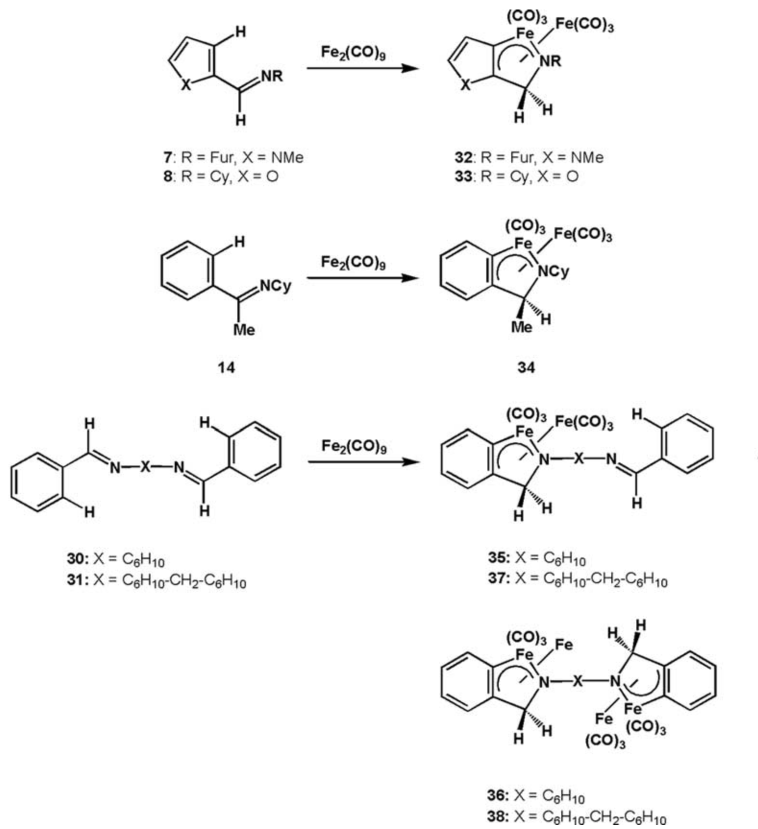

Scheme 3.

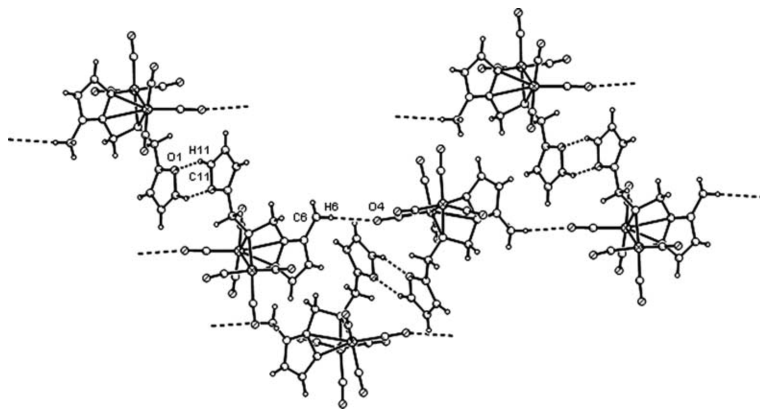

Fig. 2. Supramolecular structure of **32**, H11···O1*x* 258(1) pm, C11–H11···O1*x* 161.5(8)°, H6a···O4*x* 251(1), C6-H6a···O4*x* 172.2(8)°.

ranges from 228.1(2) pm (**33**) to 246.7(2) pm (**35**). In addition, the iron iron bond lengths also shows different values ranging from 241.24(4) pm (**35**) to 245.51(4) pm (**34**). Compared to the standard deviations these differences are unequivocally significant. These findings will be discussed in detail together with the structural data of another 39 compounds showing the same coordination mode as **32**–**35**.

The supramolecular arrangement of **32**–**35** is depicted in Figs. 2, 4, 6 and 8. The architecture of the crystal structures is determined by weak C–H···O interactions [32], which of course are highly dependent on the nature of the organic substituents attached to the ligand. If these substituents are hydrocarbon groups, the most effective hydrogen bond acceptors are the terminal CO ligands. In the case of the crystal structure of **32** the furan system in the side chain acts as an additional hydrogen bond acceptor site leading to the formation of dimers linked by a C–H···O interaction between the furan oxygen and a hydrogen atom of the furan moiety of a neighboring molecule and vice versa. These dimers are connected to infinite chains by a C–H···O interaction between a CO ligand and one of the hydrogen atoms of the NMe group (Fig. 2). The supramolecular structures of **33** and **34** are quite similar in that the shortest intermolecular distances correspond to C–H···O interactions between a terminal CO and a proton of the methylene group (**33**) or the cyclohexyl substituent (**34**) building up infinite chains (Figs. 4 and 6). In the crystal structure of **35** three short C–H···O interactions are recognized, the imine nitrogen atom N2 is not involved in any hydrogen bond network. Fig. 8 shows the infinite two dimensional plain built up by the shortest intermolecular hydrogen bonds between terminal CO ligands and an aromatic hydrogen atom and one of the hydrogen atoms of the central cyclohexyl moiety. The third interaction, that has been omitted for the sake of clarity, leads to an three dimensional network by another C–H···O bond between a CO ligand and another hydrogen atom of the cyclohexyl ring.

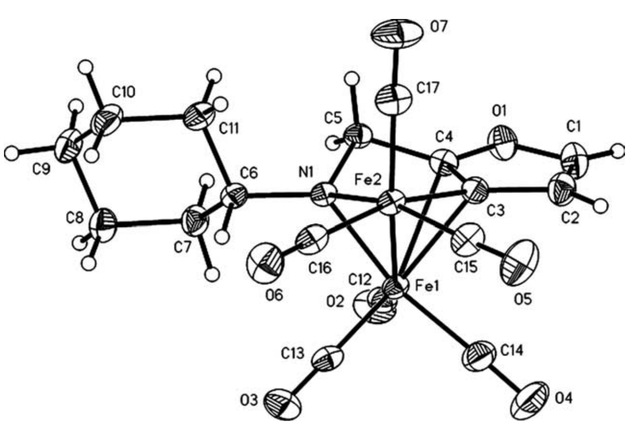

Fig. 3. Molecular structure of **33**, selected bond lengths (pm) and bond angles (°): Fe1–Fe2 244.93(5), Fe1–N1 196.8(2), Fe1–C3 216.8(2), Fe1–C4 228.1(2), Fe2–N1 200.5(2), Fe2–C3 194.8(2), C3–C4 138.4(3), C4–C5 148.5(3), C5–N1 149.0(2); N1–Fe1–Fe2 51.25(5), N1–Fe1–C3 74.62(7), N1–Fe1–C4 63.00(7), Fe2–Fe1–C3 49.45(6), Fe2–Fe1–C4 71.95(5), C3–Fe1–C4 36.15(8), N1–Fe2–C3 78.87(8), Fe2–C3–C4 112.1(2), C3–C4–C5 120.1(2), C4–C5–N1 97.4(2), C5–N1–Fe2 112.2(1).

The iron iron bond lengths as well as the iron carbon bond lengths between the apical iron atom and C_β (Scheme 1) of 43 molecular structures that have been obtained in our group during the last years are summarized in Table 1. Fig. 9 shows the correlation between the two bond lengths. The iron carbon distances in particular show a very broad range from ≈220 up to ≈268 pm, which is already above the sum of the van der Waals radii of iron and carbon. Scheme 4 shows three mesomeric

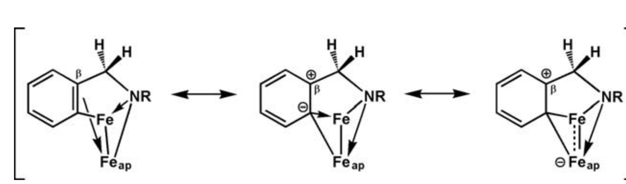

Scheme 4.

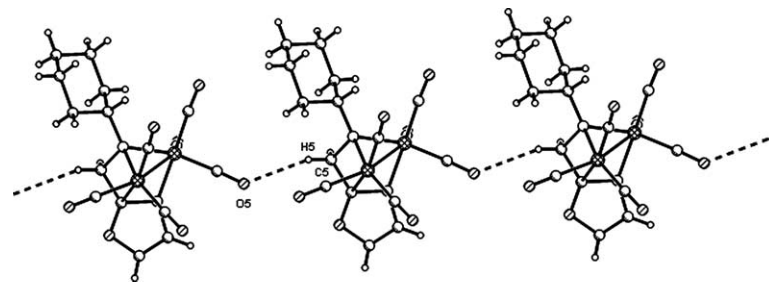

Fig. 4. Supramolecular structure of **33**, H5b···O5*x* 267.5(7) pm, C5-H5b···O5*x* 157.5(4)°.

forms of the coordination mode in the corresponding dinuclear cluster compounds that reflect the observed bonding situation on the basis of simple localized Lewis formulae. It is obvious from Scheme 4 that the longer the iron carbon bond length Fe_{ap}–C_{β} gets, the shorter becomes the iron iron bond.

The compounds with the longest iron carbon distances are the dinuclear iron carbonyl clusters derived from the ligands **22** and **23** based on β-naphthylcarbaldehyde. If the second aromatic ring of the naphthaline system is coordinated by another $Fe(CO)_3$ moiety in a η^4-fashion, the Fe_{ap}–C_{β} bond is shortened by ≈20 pm whereas the iron iron bond is elongated by ≈2 pm [10]. This example shows that the electronic properties of the corresponding aromatic system the ligands are based upon play the most important role in the observed reciprocal dependency of the bond lengths in dinuclear iron carbonyl compounds of this kind.

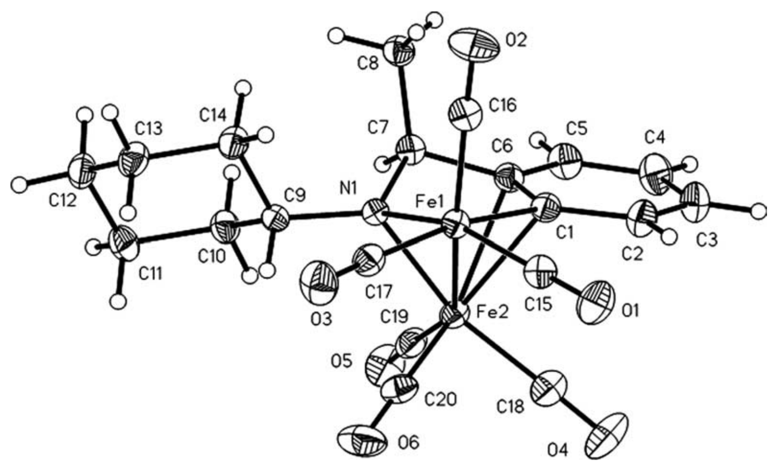

Fig. 5. Molecular structure of **34**, selected bond lengths (pm) and bond angles (°): Fe1–Fe2 245.51(4), Fe2–N1 198.8(2), Fe2–C1 218.7(2), Fe2–C6 231.5(2), Fe1–N1 200.2(2), Fe1–C1 199.2(2), C1–C6 142.5(3), C6–C7 151.8(3), C7–N1 150.4(3); N1–Fe2–Fe1 52.29(5), N1–Fe2–C1 74.47(8), N1–Fe2–C6 64.71(8), Fe1–Fe2–C1 50.41(6), Fe1–Fe2–C6 74.53(6), C1–Fe2–C6 36.76(8), N1–Fe1–C1 78.65(8), Fe1–C1–C6 114.6(2), C1–C6–C7 115.5(2), C6–C7–N1 100.3(2), C7–N1–Fe1 113.8(1).

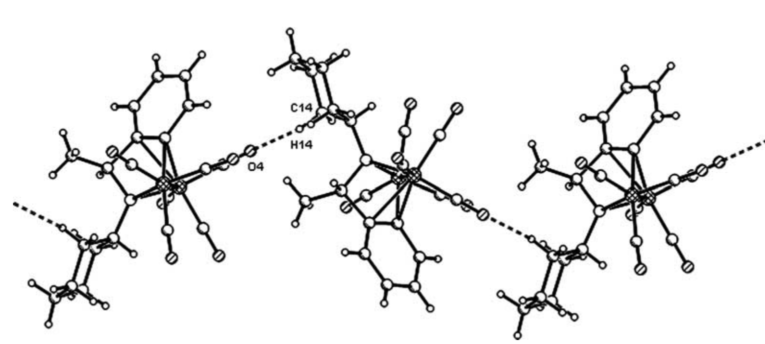

Fig. 6. Supramolecular structure of **34**, H14a···O4*x* 261.7(8) pm, C14–H14a···O4*x* 126.1(5)°.

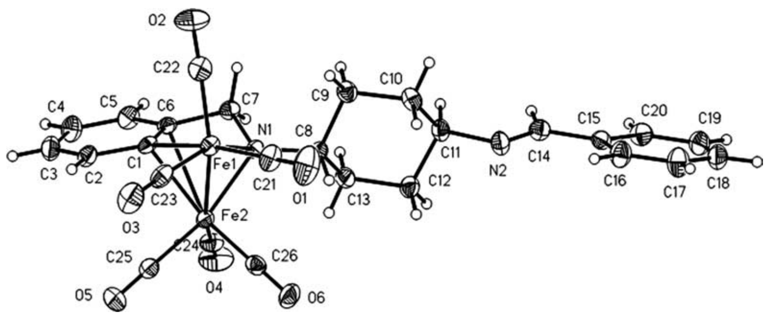

Fig. 7. Molecular structure of **35**, selected bond lengths (pm) and bond angles (°): Fe1–Fe2 241.24(4), Fe2–N1 196.3(2), Fe2–C1 217.6(2), Fe2–C6 246.7(2), Fe1–N1 198.0(2), Fe1–C1 200.6(2), C1–C6 141.3(3), C6–C7 149.8(3), C7–N1 148.3(2), C14-N2 125.3(3); N1–Fe2–Fe1 52.61(5), N1–Fe2–C1 74.52(7), N1–Fe2–C6 61.95(6), Fe1–Fe2–C1 51.55(5), Fe1–Fe2–C6 72.05(5), C1–Fe2–C6 34.74(7), N1–Fe1–C1 78.08(7), Fe1–C1–C6 113.0(1), C1–C6–C7 115.1(2), C6–C7–N1 102.2(2), C7–N1–Fe1 111.3(1), C11–N2–C14 118.3(2), N2–C14–C15 123.4(2).

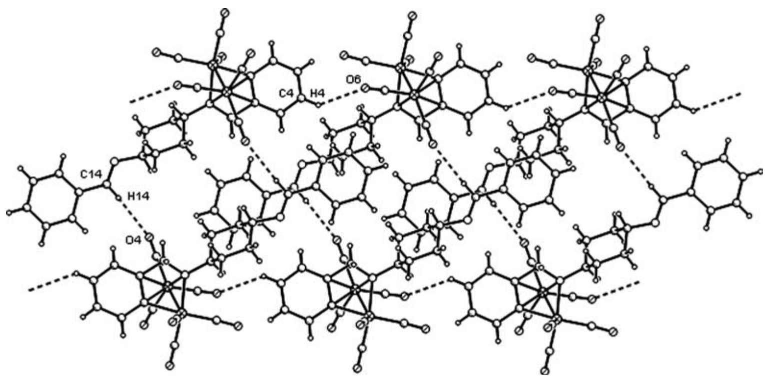

Fig. 8. Supramolecular structure of **35**, H4· · ·O6 259.8(8) pm, C4-H4· · ·O6*x* 136.6(4)°, H14· · ·O4*x* 262.9(8) pm, C14–H14· · ·O6*x* 173.8(5)°, the third C–H· · ·O interaction (H11· · ·O5*x* 263.5(8) pm, C11–H11· · ·O5*x* 135.5(5)°) has been omitted for the sake of clarity.

Another interesting feature is the reaction pathway being observed in ruthenium catalyzed C–H activation reactions in the presence of alkenes and/or carbon monoxide if the imine ligands **1**–**31** are used as the substrates. In all cases we investigated up to now the C–H activation reaction takes place at the same position that was observed in the formation of the iron carbonyl model compounds. But it is remarkable that the imines showing very long Fe_{ap}–C_{β} interactions in their iron carbonyl complexes produce heterocyclic products if reacted with carbon monoxide and ethylene (Scheme 5, Fig. 9) [16], whereas the ligands derived from benzaldimines **10**–**16** or α-naphthylcarbaldimines **18**, **19** and **21** either yield the alkene insertion products or acylated compounds by the subsequent insertion of CO and an alkene under similar reaction conditions [16,25,26,36]. The diironhexacarbonyl complexes produced from the latter ligands show Fe_{ap}–C_{β} bond lengths in the range of 228–240 pm. The only exception to this rule is the iron complex of **17** with a Fe_{ap}–C_{β} bond length of 247.4 pm but a iron iron bond which is shorter compared to the model compounds of ligands which in catalytic reactions produce heterocycles.

In Scheme 5, the isoindolone derivatives that are observed as the products of catalytic three component reactions of the imines **22**, **23**, **30** and **31** are presented.

The β-naphthyl-carbaldimines **22** and **23** show the typical reaction pathway of producing an acyl substituent by the subsequent insertion of carbon monoxide and ethylene at C-3. In addition, the insertion of another equivalent of CO into the C–H bond at C-1 is followed by the formation of a 2,9-dihydro-benzoisoindol-1-one system. One molecule of ethylene is then catalytically attached to the same naphthalene carbon atom [16]. This incorporation of two equivalents of carbon monoxide and two equivalents of ethylene takes place regioselectively meaning that the propionyl group is never observed at C-1 of the naphthalene system and the heterocycle is always formed between the positions C-1 and C-2 of the naphthalene ring. The diimines **30** and **31** also produce isoindolone derivatives under the same reaction condidtions. But in contrast to the formation of **39** and **40**, **41**–**43** are 2,3-dihydroisoindol-1-one derivatives. This means that after the insertion of CO into the C–H bond in *ortho*-position with respect to the imine substituent and the formation of the heterocyclic system, ethylene is catalytically attached to the former imine car-

Table 1
Comparison of the bond lengths Fe–Fe and Fe_{ap}–C_{β} (pm) in diironhexacarbonyl complexes showing an μ_2-η^3-enylamido ligand

Ligand	Fe–Fe	Fe_{ap}–C_{β}	Reference	Remarks
1	245.9	219.9	[5]	
2	243.4	227.9	[5]	
3	245.0	228.0	[5]	
4	242.1	247.5	[5]	
5	242.1	241.4	[5]	
6	244.0	236.4	[6]	
7	241.6	243.8	–	This paper, **32**
8	244.9	228.1	–	This paper, **33**
9	245.4	232.1	[33]	Two molecules per asymmetric unit
	245.7	227.0		
10	246.1	231.0	[9]	
11	244.1	233.6	[9]	
12	243.5	234.7	[9]	
13	244.6	237.0	[9]	
14	245.5	231.5	–	This paper, **34**
15	245.8	232.9	[34]	
16	246.0	231.1	[34]	Coordination of sulfur at Fe_{ap}
17	243.4	247.4	[35]	
18	245.3	230.3	[10]	Two molecules per asymmetric unit
	245.3	229.7		
19	244.7	230.2	[10]	
20	245.7	228.9	[36]	
21	243.7	227.4	[36]	
22	238.9	268.0	[10]	
22	242.3	245.4	[10]	Naphthaline system η^4-coordinated by another $Fe(CO)_3$ moiety
23	240.5	258.6	[10]	
23	242.9	244.6	[10]	Naphthaline system η^4-coordinated by another $Fe(CO)_3$ moiety
24	246.1	229.5	[11]	Only one imine function coordinated
24	244.0	241.4	[11]	Both imine functions coordinated, centrosymmetric molecular structure
25	242.5	236.4	[11]	Only one imine function coordinated
25	245.1	220.5	[11]	Second imine function coordinated differently
26	245.4	234.2	[12]	Only one imine function coordinated, 2 molecules per asymmetric unit
	246.7	231.6		
26	245.4	238.2	[12]	Both imine functions coordinated, centrosymmetric molecular structure
27	244.9	238.5	[12]	Both imine functions coordinated
	243.3	236.3		
28	244.7	233.5	[12]	Only one imine function coordinated
28	246.4	229.7	[12]	Both imine functions coordinated, 2 molecules per asymmetric unit
	246.6	232.5		
	246.4	231.0		
	246.9	229.9		
29	244.5	235.5	[12]	Only one imine function coordinated
30	241.2	246.7	–	This paper, **35**

bon atom. Complex **43** is obtained in more than 90% yield and could therefore be fully characterized by means of several spectroscopic techniques. NMR experiments unequivocally showed that first of all there is one more aliphatic CH moiety present than it would be expected if the reaction sequence was analogous to the one producing **39** and **40**. In addition, the methylene protons of the new ethyl substituent show a coupling with this CH group. Both facts are only consistent with a structural formula of **43** as depicted in Scheme 5. Compounds **41** and **42** were observed in much lower yield, but by GC-MS measurements as well as from typical resonances in the ^{13}C NMR of the crude reaction mixture, their identity as 2,3-dihydroisoindolone derivatives could be demonstrated. The signals of the carbonyl carbon atoms are observed at $\delta = 167.4$ and 168.8 ppm being in good agreement with the corresponding chemical shift in the spectrum of **43** (168.5 ppm) and related 1,5-dihydropyrrol-2-one derivatives (170–172 ppm) [37]. In contrast, **39** and **40** as well as related 1,3-dihydropyrrol-2-ones show the carbon resonance of the carbonyl function at ≈182 ppm [16,33,37–40].

In the near future, we will investigate the reaction pathways of **4**, **5** and **7** in catalytic reactions as well as the corresponding properties of **1** showing the shortest Fe_{ap}–C_{β} interaction at all. One of the iron carbonyl compounds derived from **25** also exhibits a very short Fe_{ap}–C_{β} bond length which in this case is caused by the second imine function which is also coordinated to another $Fe_2(CO)_6$ moiety [11].

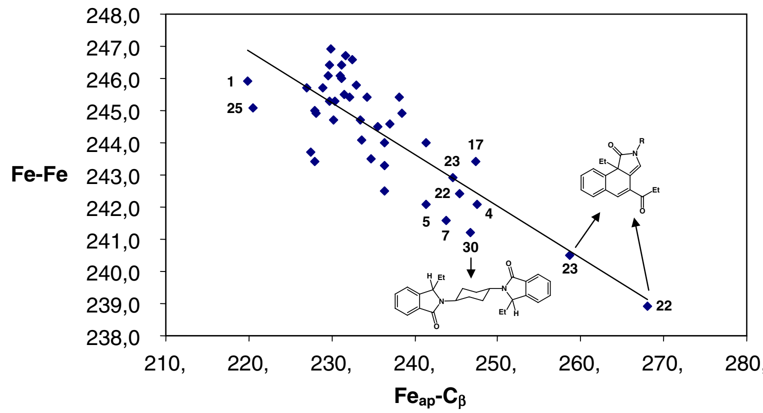

Fig. 9. Reciprocal correlation between the Fe–Fe and Fe_{ap}–$C_β$ bond lengths in dinuclear iron carbonyl complexes; the isoindolone derivatives produced by subsequent insertion of carbon monoxide and ethylene into C–H bonds of **22**, **23** and **30** are also depicted.

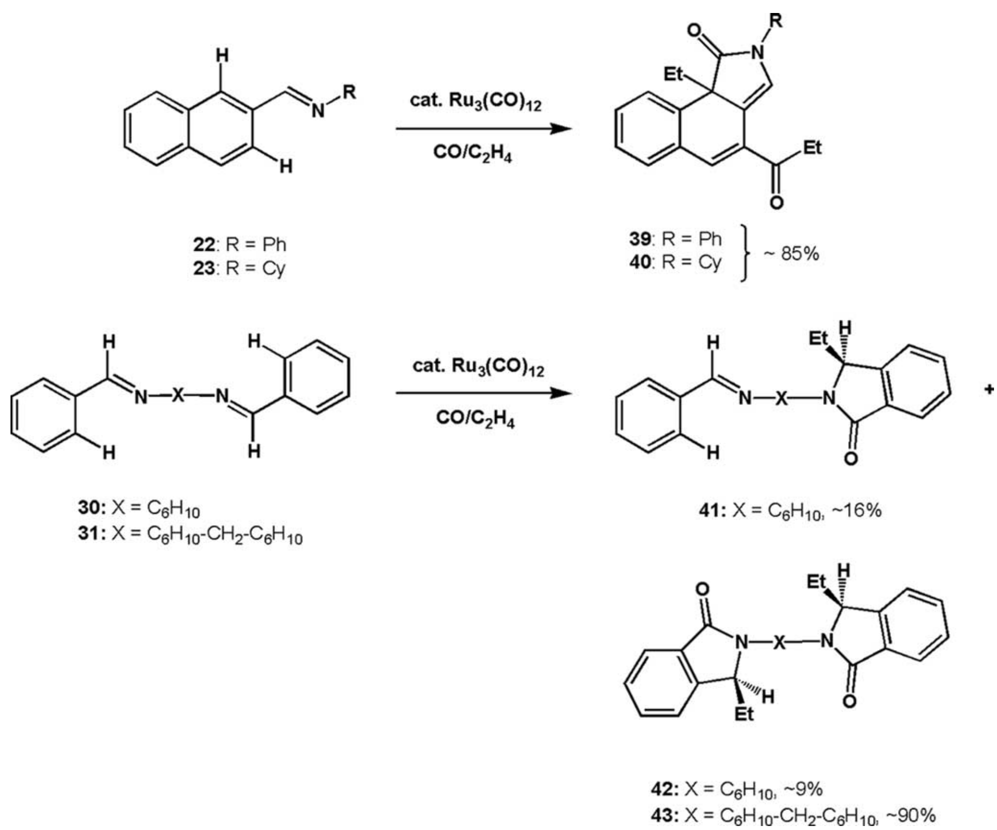

Scheme 5.

3. Experimental

3.1. General

All procedures were carried out under an argon atmosphere in anhydrous, freshly distilled solvents.

Infrared spectra were recorded on a Perkin–Elmer FT-IR System 2000 using 0.2 mm KBr cuvettes. NMR spectra were recorded on a Bruker AC 200 spectrometer (^{1}H: 200 MHz, ^{13}C: 50.32 MHz, $CDCl_3$ as internal standard). Mass spectra were recorded on a Finnigan MAT SSQ 710 instrument. Elemental analyses were carried out at the laboratory of the Institute of Oraganic Chemistry and Macromolecular Chemistry of the Friedrich-Schille-University Jena.

3.2. X-ray crystallographic studies

The structure determinations of **32** and **33** were carried out on an Enraf Nonius CAD4 diffractometer, the structure determinations of **34** and **35** were carried out on a Enraf Nonius Kappa CCD diffractometer, in all cases using graphite monochromated Mo Kα radiation. The crystal was mounted in a stream of cold nitrogen. Data were corrected for Lorentz and polarization effects but not for absorption. The structure was solved by direct methods and refined by full-matrix least-squares techniques against F^2 using the programs SHELXS-86 and SHELXL-97 [41,42]. Computation of the structures and the molecular illustrations were drawn using the program XP [43]. The crystal and intensity data are given in Table 2.

3.3. Synthesis of 7, **8** and **14**

The ligands were synthesized by literature procedures and characterized by comparison of melting points and NMR spectroscopical data with the data reported in the literature [44–46].

3.4. Synthesis of **30** and **31**

A sample of 25 mmol of the corresponding diamine (2.855 g *trans*-cyclohexane-1,4-diamine, 5.259 g 4,4′-diamino-dicyclohexylmethane) is dissolved in 100 mL of anhydrous ethanol and 5.306 g (50 mmol) benzaldehyde are added. After stirring at room temperature for 20 h the resulting precipitate is collected and washed twice with cold anhydrous ethanol and cold diethylether. The melting point of **30** was identical to the one reported in the literature [47]. Yield: 5.528 g **30** (76.1%), 2.608 **31** (27.0%).

3.5. Analytical data for **31**

MS (CI, H_2O): 387 (MH^+), 299 ($C_{20}H_{31}N_2^+$), 201 ($C_{14}H_{19}N^+$), 123 ($C_8H_{13}N^+$), 105 ($C_7H_7N^+$); IR (Nujol, cm^{-1}): 1643 s; ^1H NMR (200 MHz, $CDCl_3$, 298 K): 0.60–2.22 (m, 20H, CH, CH_2), 3.04–3.29 (m, 2H, CH), 7.28–7.50 (m, 6H, =CH), 7.64–7.82 (m, 4H, =CH), 8.32 (s, 2H, N=CH); ^{13}C NMR (200 MHz, $CDCl_3$, 298 K): 31.8 (CH_2), 33.6 (CH), 34.0 (CH_2), 44.7 (CH_2), 70.2 (CH), 127.9 (=CH), 128.3 (=CH), 130.1 (=CH), 136.4 (=C), 158.6 (N=CH). Anal. Calc. for $C_{27}H_{34}N_2$ (found) (%): C 83.89 (84.01), H 8.86 (9.04), N 7.25 (7.26).

3.6. Synthesis of **32**–**38**

A 360 mg portion $Fe_2(CO)_9$ (1 mmol) together with an equimolar amount of the corresponding imines with only one imine function (188 mg **7**, 177 mg **8**, 201 mg **14**) or half an equivalent of the diimines (146 mg **30**, 193 mg

Table 2
Crystal and intensity data for **32**, **33**, **34** and **35**

	32	33	34	35
Formula	$C_{17}H_{12}N_2O_7Fe_2$	$C_{17}H_{15}NO_7Fe_2$	$C_{20}H_{19}NO_6Fe_2$	$C_{26}H_{22}N_2O_6Fe_2$
Molecular weight (g mol^{-1})	467.99	457.00	481.06	570.16
Radiation	Mo Kα	Mo Kα	Mo Kα	Mo Kα
Monochromator	Graphite	Graphite	Graphite	Graphite
T (K)	183	183	183	183
Crystal color	Red	Red	Red	Red
Crystal size	0.4 × 0.3 × 0.3	0.2 × 0.1 × 0.1	0.2 × 0.2 × 0.1	0.5 × 0.2 × 0.1
a (Å)	7.853(4)	17.426(3)	8.5901(3)	9.8896(2)
b (Å)	11.468(6)	8.802(1)	16.6276(5)	24.201(1)
c (Å)	20.33(2)	12.175(2)	14.6971(5)	10.9304(4)
α (°)	90	90	90	90
β (°)	93.07(6)	100.27(1)	99.327(2)	104.966(2)
γ (°)	90	90	90	90
V (Å^3)	1828(2)	1837.5(5)	2071.5(1)	2527.3(2)
Z	4	4	4	4
F(000)	944	928	984	1168
ρ_{calc} (g cm^{-3})	1.700	1.652	1.543	1.498
Crystal system	Monoclinic	Monoclinic	Monoclinic	Monoclinic
Space group	$P2_1/c$	$P2_1/c$	$P2_1/c$	$P2_1/n$
Absorption coefficient (mm^{-1})	1.635	1.622	1.436	1.191
θ Limit (°)	$2.60 < \theta < 25.07$	$1.19 < \theta < 25.00$	$2.40 < \theta < 23.27$	$1.68 < \theta < 27.48$
Reflections measured	3324	4255	5529	9530
Independent reflections	3227	3247	2984	5735
R_{int}	0.1353	0.0179	0.0227	0.0312
Reflections observed ($F_o^2 > 2\sigma(F_o^2)$)	2590	2955	2623	4090
Number of parameters	301	304	338	413
Goodness-of-fit	1.085	1.046	1.026	0.970
R_1	0.0336	0.0274	0.0245	0.0354
wR_2	0.0889	0.0727	0.0585	0.0688
Final diffraction map electron density peak (e Å^{-3})	0.472	0.389	0.239	0.326

31) and 20 mL *n*-heptane are stirred together at 50 °C for 45 min. In the course of the reaction the pale yellow suspension slowly changes to a deep red solution as the ligand and $Fe_2(CO)_9$ dissolve. After the reaction is completed all volatile materials are removed in vacuo. The residue is dissolved in CH_2Cl_2, 1 g silanized silica gel is added and the solvent is again removed under reduced pressure. Chromatography on silica gel using light petroleum (b.p. 40–60 °C) as the eluent first yields a small green band containing $Fe_3(CO)_{12}$ followed by a deep red band of **32**, **33** or **34**, respectively. Chromatographic workup of the crude reaction mixture from the reaction of **30** with $Fe_2(CO)_9$ first yields a band containing the tetranuclear iron carbonyl cluster compound **36** using a mixture of light petroleum (b.p. 40–60 °C) and CH_2Cl_2 in a 2:1 ratio. Using a mixture of light petroleum (b.p. 40–60 °C) and THF in a 10:1 ratio leads to the elution of **34** as the main product of the reaction. Similarily, the chromatographic workup of the crude reaction mixture of the reaction of **31** with $Fe_2(CO)_9$ first elutes the tetranuclear cluster compound **38** (light petroleum (b.p. 40–60 °C)/CH_2Cl_2 2:1), whereas the second fraction eluted with a mixture of light petroleum (b.p. 40–60 °C) and THF in a 10:2 ratio contains the dinuclear compound **37**. Yield: 152 mg **32** (32.5%), 86 mg **33** (18.8%), 180 mg **34** (37.4%), 104 mg **35** (36.5%), 88 mg **36** (20.7%), 91 mg **37** (27.3%), 31 mg **38** (6.6%). Recrystallization of the complexes was performed from mixtures of light petroleum (b.p. 40–60 °C) and CH_2Cl_2 at −20 °C.

*3.7. Analytical data for **32***

MS (EI): 468 (M^+), loss of six CO and two Fe; IR (CH_2Cl_2, cm^{-1}): 2057 s, 2019 vs, 1972 vs (br); ^{1}H NMR (200 MHz, $CDCl_3$, 298 K): 3.61 (s, 3H, CH_3), 3.79 (s, 2H, CH_2), 3.87 (s, 2H, CH_2), 6.27 (m, 1H, =CH), 6.34 (m, 1H, =CH), 6.52 (d, $^3J_{HH}$ = 2.9 Hz, 1H, =CH), 6.86 (d, $^3J_{HH}$ = 2.9 Hz, 1H, =CH), 7.40 (s, 1H, =CH); ^{13}C NMR (200 MHz, $CDCl_3$, 298 K):35.3 (CH_3), 63.2 (CH_2), 63.5 (CH_2), 109.4 (=CH), 110.3 (=CH), 114.7 (=C), 126.7 (=CH), 131.0 (=CH), 141.7 (=C), 142.2 (=CH), 152.7 (=C), 211.5 (CO). Anal. Calc. for $C_{17}H_{12}N_2O_7Fe_2$ (found): C 43.63 (43.91), H 2.58 (2.89), N 5.99 (5.92).

*3.8. Analytical data for **33***

MS (EI): 457 (M^+), loss of six CO and two Fe; IR (CH_2Cl_2, cm^{-1}): 2065 m, 2026 vs, 1983 vs (br); ^{1}H NMR (200 MHz, $CDCl_3$, 298 K): 0.83–2.10 (m, 11H, CH_2, CH), 3.74 (s, 2H, CH_2), 6.71 (d, $^3J_{HH}$ = 1.9 Hz, 1H, =CH), 7.41 (d, $^3J_{HH}$ = 1.9 Hz, 1H, =CH); ^{13}C NMR (200 MHz, $CDCl_3$, 298 K): 25.9 (CH_2), 26.1 (CH_2), 35.8 (CH_2), 57.5 (CH_2), 74.3 (CH), 122.1 (=CH), 131.2 (=C), 138.7 (=C), 148.0 (=CH), 210.3 (CO). Anal. Calc. for $C_{17}H_{15}NO_7Fe_2$ (found): C 44.68 (45.04), H 3.31 (3.59), N 3.06 (2.95).

*3.9. Analytical data for **34***

MS (EI): 481 (M^+), loss of six CO and two Fe; IR (CH_2Cl_2, cm^{-1}): 2060 m, 2022 vs, 1982 vs (br); ^{1}H NMR (200 MHz, $CDCl_3$, 298 K): 0.78 (d, $^3J_{HH}$ = 6.1 Hz, 3H, CH_3), 0.88–2.32 (m, 11H, CH_2, CH), 4.58 (q, $^3J_{HH}$ = 6.1 Hz, 1H, CH), 6.98 (dd, $^3J_{HH}$ = 8.2 Hz, $^3J_{HH}$ = 8.2 Hz, 1H, =CH), 7.23 (dd, $^3J_{HH}$ = 8.2 Hz, $^3J_{HH}$ = 8.2 Hz, 1H, =CH), 7.51 (d, $^3J_{HH}$ = 8.2 Hz, 1H, =CH), 8.02 (d, $^3J_{HH}$ = 8.2 Hz, 1H, =CH); ^{13}C NMR (200 MHz, $CDCl_3$, 298 K): 26.4 (CH_2), 26.8 (CH_3), 27.1 (CH_2), 28.6 (CH_2), 36.9 (CH_2), 41.1 (CH_2), 72.3 (CH), 76.6 (CH), 118.9 (=C), 120.9 (=C), 125.7 (=CH), 129.9 (=CH), 130.2 (=CH), 149.2 (=CH), 210.4 (CO). Anal. Calc. for $C_{20}H_{19}NO_6Fe_2$ (found): C 49.93 (50.05), H 3.98 (4.32), N 2.91 (2.89).

*3.10. Analytical data for **35***

MS (FAB in NBA): 571 (MH^+), loss of six CO; HRMS (FAB in NBA) calcd. for $C_{26}H_{23}N_2O_6Fe_2$ (MH^+) 571.0292, found 571.0273, Δ = 1.90 mmu. IR (CH_2Cl_2, cm^{-1}): 2060 s, 2055 s, 2023 vs, 1984 vs, 1977 vs, 1971 sh, 1961 vs, 1948 vs (br), 1644 m; ^{1}H NMR (200 MHz, $CDCl_3$, 298 K): 1.55–2.13 (m, 8H, CH_2), 2.30–2.63 (m, 1H, CH), 2.94–3.35 (m, 1H CH), 3.95 (s, 2H, CH_2), 7.04 (dd, $^3J_{HH}$ = 7.0 Hz, $^3J_{HH}$ = 7.0 Hz, 1H, =CH), 7.30 (dd, $^3J_{HH}$ = 7.5 Hz, $^3J_{HH}$ = 7.5 Hz, 1H, =CH), 7.34–7.60 (m, 4H, =CH), 7.60–7.83 (m, 2H, =CH), 8.10 (d, $^3J_{HH}$ = 8.0 Hz, 1H, =CH), 8.29 (s, 1H, N=CH); ^{13}C NMR (200 MHz, $CDCl_3$, 298 K): 33.1 (CH_2), 33.5 (CH_2), 64.9 (CH), 69.3 (CH), 73.3 (CH_2), 125.2 (=C), 125.7 (=CH), 128.1 (=CH), 128.6 (=CH), 130.6 (=CH), 136.3 (=C), 145.5 (=CH), 151.0 (=C), 159.5 (N=CH), 210.5 (CO).

*3.11. Analytical data for **36***

MS (FAB in NBA): 850 (M^+), loss of 12 CO; HRMS (FAB in NBA) calcd. for $C_{32}H_{22}N_2O_{12}Fe_4$ (M^+) 849.9200, found 849.9231, Δ = 3.10 mmu. IR (nujol, cm^{-1}): 2059 vs, 2020 vs, 1990 vs, 1975 vs, 1962 vs, 1957 vs (br), 1925 vs (br); ^{1}H NMR (200 MHz, $CDCl_3$, 298 K): 1.44–2.08 (m, 8H, CH_2), 2.12–2.42 (m, 2H, CH), 3.89 (s, 4H, CH_2), 7.04 (dd, $^3J_{HH}$ = 7.5 Hz, $^3J_{HH}$ = 7.5 Hz, 2H, =CH), 7.30 (dd, $^3J_{HH}$ = 7.4 Hz, $^3J_{HH}$ = 7.4 Hz, 2H, =CH), 7.47 (d, $^3J_{HH}$ = 7.9 Hz, 2H, =CH), 8.08 (d, $^3J_{HH}$ = 8.1 Hz, 2H, =CH); ^{13}C NMR (200 MHz, $CDCl_3$, 298 K): 33.7 (CH_2), 64.8 (CH), 73.4 (CH_2), 125.6 (=C), 125.8 (=CH), 128.1 (=CH), 130.9 (=CH), 145.2 (=CH), 151.0 (=C), 210.4 (CO).

3.12. Analytical data for **37**

MS (FAB in NBA): 667 (MH^+), loss of six CO; HRMS (FAB in NBA) calcd. for $C_{33}H_{35}N_2O_6Fe_2$ (MH^+) 667.3433, found 667.3418, $\Delta = -1.54$ mmu. IR (nujol, cm^{-1}): 2060 vs, 2022 vs, 1977 vs (br), 1644 w; ^1H NMR (200 MHz, $CDCl_3$, 298 K): 0.70–2.16 (m, 20H, CH, CH_2), 2.16–2.53 (m, 1H, CH), 3.00–3.34 (m, 1H, CH), 3.91 (s, 2H, CH_2), 7.02 (dd, $^3J_{HH} = 7.5$ Hz, $^3J_{HH} = 7.5$ Hz, 1H, =CH), 7.27 (dd, $^3J_{HH} = 7.0$ Hz, $^3J_{HH} = 7.0$ Hz, 1H, =CH), 7.33–7.58 (m, 4H, =CH), 7.61–7.80 (m, 2H, =CH), 8.08 (d, $^3J_{HH} = 8.1$ Hz, 1H, =CH), 8.30 (s, 1H, N=CH); ^{13}C NMR (200 MHz, $CDCl_3$, 298 K): 31.9 (CH_2), 32.9 (CH_2), 33.9 (CH), 34.1 (CH_2), 34.5 (CH_2), 34.9 (CH_2), 44.1 (CH_2), 64.8 (CH), 70.4 (CH), 74.4 (CH_2), 125.0 (=C), 125.6 (=CH), 128.0 (=CH), 128.1 (=CH), 128.5 (=CH), 130.3 (=CH), 130.5 (=CH), 136.6 (=C), 145.7 (=CH), 150.9 (=C), 158.8 (N=CH), 210.6 (CO).

3.13. Analytical data for **38**

MS (FAB in NBA): 946 (MH^+), loss of 12 CO; HRMS (FAB in NBA) calcd. for $C_{34}H_{35}N_2O_7Fe_4$ ($MH^+ - 5CO$) 807.0477, found 807.0441, $\Delta = -3.58$ mmu. IR (nujol, cm^{-1}): 2065 vs, 2024 vs, 2006 vs, 1988 vs (br), 1975 vs (br), 1959 vs (br), 1953 vs (sh), 1940 vs (br); ^1H NMR (200 MHz, $CDCl_3$, 298 K): 1.65–2.06 (m, 20H, CH, CH_2), 2.06–2.50 (m, 2H, CH), 3.91 (s, 4H, CH_2), 7.03 (dd, $^3J_{HH} = 6.9$ Hz, $^3J_{HH} = 6.9$ Hz, 2H, =CH), 7.28 (dd, $^3J_{HH} = 6.9$ Hz, $^3J_{HH} = 6.9$ Hz, 2H, =CH), 7.46 (d, $^3J_{HH} = 7.9$ Hz, 2H, =CH), 8.08 (d, $^3J_{HH} = 8.1$ Hz, 2H, =CH); ^{13}C NMR (200 MHz, $CDCl_3$, 298 K): 32.8 (CH_2), 34.6 (CH), 34.9 (CH_2), 43.4 (CH_2), 64.8 (CH), 74.3 (CH_2), 125.1 (=C), 125.6 (=CH), 128.1 (=CH), 130.5 (=CH), 145.7 (=CH), 150.9 (=C), 210.6 (CO).

3.14. Synthesis of **41**–**43**

In a typical reaction a 50 mL autoclave charged with 1 mmol of the corresponding diimine (290 mg **30**, 386 mg **31**), $Ru_3(CO)_{12}$ (0.03 mmol) and toluene (5 mL) was pressurized with carbon monoxide (12 bar) and ethylene (8 bar) and heated at 145 °C overnight. After the reaction mixture was cooled to room temperature it was transferred to a Schlenk tube and all volatile material was removed under reduced pressure. The remaining oily residue was used for NMR and IR spectroscopy and GC-MS measurements.

3.15. Analytical data for **41**

MS (EI): 346 (M^+), 318 ($C_{22}H_{26}N_2^+$), 241 ($C_{16}H_{21}N_2^+$), 226 ($C_{15}H_{18}N_2^+$), 214 ($C_{14}H_{18}N_2^+$), 202 ($C_{13}H_{18}N_2^+$), 185 ($C_{13}H_{15}N^+$), 162 ($C_{10}H_{14}N_2^+$), 145 ($C_{10}H_{11}N^+$), 132 ($C_9H_{10}N^+$), 117 ($C_9H_9^+$), 104 ($C_7H_6N^+$), 91 ($C_7H_7^+$), 81 ($C_6H_9^+$); HRMS (ESI in $CHCl_3$/methanol): calcd. for $C_{23}H_{26}N_2ONa$ (MNa^+) 369.4610, found 369.4608, $\Delta = -0.23$ mmu.

3.16. Analytical data for **42**

MS (EI): 402 (M^+), 297 ($C_{20}H_{29}N_2^+$), 282 ($C_{19}H_{26}N_2^+$), 270 ($C_{18}H_{26}N_2^+$), 242 ($C_{17}H_{24}N^+$), 218 ($C_{15}H_{24}N^+$), 202 ($C_{14}H_{20}N^+$), 185 ($C_{13}H_{15}N^+$), 172 ($C_{12}H_{14}N^+$), 156 ($C_{11}H_{10}N^+$), 132 ($C_9H_{10}N^+$), 117 ($C_9H_9^+$), 104 ($C_8H_8^+$), 91 ($C_7H_7^+$), 81 ($C_6H_9^+$), 51 ($C_4H_3^+$); HRMS (ESI in $CHCl_3$/methanol) calcd. for $C_{26}H_{30}N_2O_2Na$ (MNa^+) 425.5250, found 425.5242, $\Delta = -0.79$ mmu.

3.17. Analytical data for **43**

MS (CI, H_2O): 499 (MH^+), 483 ($C_{32}H_{39}N_2O_2^+$), 469 ($C_{31}H_{37}N_2O_2^+$), 443 ($C_{30}H_{39}N_2O^+$), 355 ($C_{25}H_{27}N_2^+$), 338 ($C_{25}H_{24}N^+$), 267 ($C_{19}H_{25}N^+$), 243 ($C_{17}H_{25}N^+$), 189 ($C_{13}H_{19}N^+$), 175 ($C_{12}H_{17}N^+$), 161 ($C_{11}H_{15}N^+$), 147 ($C_{10}H_{13}N^+$), 145 ($C_{10}H_{11}N^+$), 123 ($C_8H_{13}N^+$), 105 ($C_7H_7N^+$); HRMS (ESI in $CHCl_3$/methanol) calcd. for $C_{33}H_{42}N_2O_2Na$ (MNa^+) 521.6968, found 521.6975, $\Delta = 0{,}69$ mmu; ^1H NMR ($CDCl_3$, 298 K) (ppm): 0.52 (t, $^3J_{HH} = 7{,}0$ Hz, 6H, CH_3), 0.68–2.19 (m, 24H, CH, CH_2), 3.63–3.97 (m, 2H, CH), 4.53–4.72 (m, 2H, CH–N), 7.22–7.85 (m, 8H, CH_{ar}); ^{13}C NMR ($CDCl_3$, 298 K) (ppm): 6.0 (CH_3), 24.7 (CH_2), 29.9 (CH_2), 30.5 (CH_2), 32.4 (CH_2), 32.5 (CH_2), 32.6 (CH_2), 32.7 (CH_2), 33.6 (CH), 44.0 (CH_2), 53.1 (CH), 59.8 (CH–N), 121.4 (=CH), 122.9 (=CH), 127.5 (=CH), 130.8 (=CH), 133.0 (=C), 144.8 (=C), 168.5 (CO).

4. Supplementary material

Additional material on the structure analyses is available from the Cambridge Crystallographic Data Centre by mentioning the deposition number CCDC-243098 (**32**), CCDC-243099 (**33**), CCDC-243100 (**34**), CCD-243101 (**35**).

References

[1] M.M. Bagga, P.L. Pauson, F.J. Preston, R.I. Reed, J. Chem. Soc., Chem. Commun. (1965) 543.
[2] P.E. Baikie, O.S. Mills, J. Chem. Soc., Chem. Commun. (1966) 707.
[3] M.M. Bagga, W.T. Flannigan, G.R. Knox, P.L. Pauson, F.J. Preston, R.I. Reed, J. Chem. Soc. (C) (1968) 36.
[4] W.T. Flannigan, G.R. Knox, P.L. Pauson, F.J. Preston, J. Chem. Soc. (C) (1969) 2077.
[5] W. Imhof, J. Organomet. Chem. 533 (1997) 31.
[6] W. Imhof, J. Organomet. Chem. 541 (1997) 109.
[7] D.-L. Wang, W.-S. Hwang, L.-C. Liang, L.-I. Wang, L. Lee, M.Y. Chiang, Organometallics 16 (1997) 3109.

[8] W.-S. Hwang, D.-L. Wang, M.Y. Chiang, J. Organomet. Chem. 613 (2000) 231.
[9] W. Imhof, A. Göbel, D. Ohlmann, J. Flemming, H. Fritzsche, J. Organomet. Chem. 584 (1999) 33.
[10] W. Imhof, Organometallics 18 (1999) 4845.
[11] W. Imhof, A. Göbel, J. Organomet. Chem. 610 (2000) 102.
[12] A. Göbel, G. Leibeling, M. Rudolph, W. Imhof, Organometalllics 22 (2003) 759.
[13] Y.-F. Tzeng, C.-Y. Wu, W.-S. Hwang, C.-H. Hung, J. Organomet. Chem. 687 (2003) 16.
[14] H.-J. Knölker, E. Baum, P. Gonser, G. Rohde, H. Röttele, Organometallics 17 (1998) 3916.
[15] S. Murai, F. Kakiuchi, S. Sekine, Y. Tanaka, A. Kamatani, M. Sonoda, N. Chatani, Nature 366 (1993) 529.
[16] D. Berger, W. Imhof, Tetrahedron 56 (2000) 2015.
[17] D. Berger, A. Göbel, W. Imhof, J. Mol. Catal. A 165 (2001) 37.
[18] T. Fukuyama, N. Chatani, F. Kakiuchi, S. Murai, J. Org. Chem. 62 (1997) 5647.
[19] F. Kakiuchi, S. Murai, Acc. Chem. Res. 35 (2002) 826.
[20] S. Murai, F. Kakiuchi, S. Sekine, Y. Tanaka, A. Kamatani, M. Sonoda, N. Chatani, Pure Appl. Chem. 66 (1994) 1527.
[21] F. Kakiuchi, S. Sekine, Y. Tanaka, A. Kamatani, M. Sonoda, N. Chatani, S. Murai, Bull. Chem. Soc. Jpn. 68 (1995) 62.
[22] M. Sonoda, F. Kakiuchi, N. Chatani, S. Murai, J. Organomet. Chem. 504 (1995) 151.
[23] M. Sonoda, F. Kakiuchi, N. Chatani, S. Murai, Bull. Chem. Soc. Jpn. 70 (1997) 3117.
[24] S. Murai, N. Chatani, F. Kakiuchi, Pure Appl. Chem. 69 (1997) 589.
[25] F. Kakiuchi, M. Yamauchi, N. Chatani, S. Murai, Chem. Lett. (1996) 111.
[26] F. Kakiuchi, T. Sato, T. Tsujimoto, M. Yamauchi, N. Chatani, S. Murai, Chem. Lett. (1998) 1053.
[27] F. Kakiuchi, M. Sonoda, T. Tsujimoto, N. Chatani, S. Murai, Chem. Lett. (1999) 1083.
[28] F. Kakiuchi, T. Tsujimoto, M. Sonoda, N. Chatani, S. Murai, Synlett (2001) 948.
[29] F. Kakiuchi, T. Sato, K. Igi, N. Chatani, S. Murai, Chem. Lett. (2001) 386.
[30] M. Sonoda, F. Kakiuchi, A. Kamatani, N. Chatani, S. Murai, Chem. Lett. (1996) 109.
[31] F. Kakiuchi, H. Ohtaki, M. Sonoda, N. Chatani, S. Murai, Chem. Lett. (2001) 918.
[32] G.R. Desiraju, T. Steiner, The Weak Hydrogen Bond, Oxford Science Publications, Oxford, 1999.
[33] W. Imhof, D. Berger, Acta Crystallogr. Sect. E 60 (2004) m384.
[34] W. Imhof, A. Göbel, L. Schweda, H. Görls, Polyhedron (2005) submitted.
[35] D. Dönnecke, K. Halbauer, W. Imhof, J. Organomet. Chem. 689 (2004) 2707.
[36] D. Dönnecke, J. Wunderle, W. Imhof, J. Organomet. Chem. 689 (2004) 585.
[37] T. Morimoto, N. Chatani, S. Murai, J. Am. Chem. Soc. 121 (1999) 1758.
[38] D. Berger, W. Imhof, Chem. Commun. (1999) 1457.
[39] W. Imhof, D. Berger, M. Kötteritzsch, M. Rost, B. Schönecker, Adv. Synth. Catal. 343 (2001) 795.
[40] D. Dönnecke, W. Imhof, Tetrahedron 59 (2003) 8499.
[41] G. Sheldrick, SHELXS-86, Universität Göttingen, Göttingen, Germany, 1986.
[42] G. Sheldrick, SHELXL-97, Universität Göttingen, Göttingen, Germany, 1997.
[43] Siemens Analytical Xray Inst. Inc., XP – Interactive Molecular Graphics, Vers. 4.2, 1990.
[44] R.C. Commes, A. Gaset, J.P. Gorrichon, G. Michel, Eur. J. Med. Chem. 13 (1978) 527.
[45] P. Devi, J.S. Sandhu, G. Thyagarajan, J. Heterocycl. Chem. 16 (1979) 1073.
[46] J.M. Ruxer, A. Solladie-Cavallo, G. Solladie, D. Olliero, Org. Magn. Res. 10 (1977) 105.
[47] N.E. Agafonov, G.Y. Kondrat'eva, V.S. Bogdanov, Bull. Acad. Sci. USSR Div. Chem. Sci. (Engl. Trans.) 37 (1988) 715.